ADVANCED MATERIALS
www.advmat.de

Check for updates

W-Based Atomic Laminates and Their 2D Derivative $W_{1.33}C$ MXene with Vacancy Ordering

*Rahele Meshkian, Martin Dahlqvist, Jun Lu, Björn Wickman, Joseph Halim, Jimmy Thörnberg, Quanzheng Tao, Shixuan Li, Saad Intikhab, Joshua Snyder, Michel W. Barsoum, Melike Yildizhan, Justinas Palisaitis, Lars Hultman, Per O. Å. Persson, and Johanna Rosen**

Structural design on the atomic level can provide novel chemistries of hybrid MAX phases and their MXenes. Herein, density functional theory is used to predict phase stability of quaternary *i*-MAX phases with in-plane chemical order and a general chemistry $(W_{2/3}M^2_{1/3})_2AC$, where M^2 = Sc, Y (W), and A = Al, Si, Ga, Ge, In, and Sn. Of over 18 compositions probed, only two—with a monoclinic C2/c structure—are predicted to be stable: $(W_{2/3}Sc_{1/3})_2AlC$ and $(W_{2/3}Y_{1/3})_2AlC$ and indeed found to exist. Selectively etching the Al and Sc/Y atoms from these 3D laminates results in $W_{1.33}C$-based MXene sheets with ordered metal divacancies. Using electrochemical experiments, this MXene is shown to be a new, promising catalyst for the hydrogen evolution reaction. The addition of yet one more element, W, to the stable of M elements known to form MAX phases, and the synthesis of a pure W-based MXene establishes that the etching of *i*-MAX phases is a fruitful path for creating new MXene chemistries that has hitherto been not possible, a fact that perforce increases the potential of tuning MXene properties for myriad applications.

The quest for, and interest in, novel 2D materials, like graphene, has increased tremendously in the last decade, motivated, in most part, by diverse applications such as memory devices, flexible electronics, and energy storage.[1] The family of 2D materials has grown to include metals, semiconductors, and insulators, exemplified by $NbSe_2$, MoS_2, and hBN, respectively. Discovered in 2011, a new class of 2D materials, MXenes, were obtained by selective etching of A-group elements, typically Al, from the atomically laminated parent $M_{n+1}AX_n$ (MAX) phases, where M is an early transition metal, A is an A-group element (mostly 13 and 14), and X is C and/or N.[2,3] MXenes show a wide range of applications, from energy storage,[4] to cationic adsorption,[5] and electromagnetic interference shielding,[6] amongst many others. In general, MXenes display quite promising, and sometimes record-setting performances.

When the A-element is etched, it is replaced by surface terminations, T_x, and hence the proper MXene formula is $M_{n+1}X_nT_x$, where T_x is a combination of −O, −OH, and −F.[7] MXenes stand out in several ways and offer key advantages over other 2D materials, in particular, their chemical diversity and tailorability, allowing for systematic variations of both their intrinsic compositions, as well as by modifying their surface terminations. However, even though there are more than 20 MXenes known to date, a quest since their discovery has been to extend MXene chemistries beyond the traditional MAX phase elements.[2]

The driving force to search for new elements is clear; with more elements to choose from, the larger the range of attainable properties. There have been no reports to date of MAX phases or MXenes with tungsten, W.[2] It is, however, well established that the W−C bond is one of the strongest known. Theory predicts that a WC-based MXene should be a topological insulator[8] or an effective catalyst.[9] W-based compounds display high thermal and electrical conductivities, excellent high-temperature strengths, low thermal expansions, and vapor pressures as well as good resistance to thermal shock. Known 2D W-based materials are the direct bandgap semiconductors WSe_2 and WS_2, which are promising candidates for electronics and optoelectronics due to their high charge carrier mobilities.[10,11] WS_2/graphene heterostructures have also shown the highest on/off ratio for graphene-based transistor devices.[12]

Currently, the best catalyst for the hydrogen, H_2, evolution reaction (HER) is platinum which is expensive. New and

R. Meshkian, Dr. M. Dahlqvist, Dr. J. Lu, Dr. J. Halim, J. Thörnberg, Q. Tao, Dr. M. Yildizhan, Dr. J. Palisaitis, Prof. L. Hultman, Prof. P. O. Å. Persson, Prof. J. Rosen
Thin Film Physics Division
Department of Physics
Chemistry and Biology (IFM)
Linköping University
SE-581 83 Linköping, Sweden
E-mail: johanna.rosen@liu.se

Dr. B. Wickman
Chemical Physics
Department of Physics
Chalmers University of Technology
SE-412 96 Gothenburg, Sweden

S. Li, S. Intikhab, J. Snyder
Department of Chemical and Biological Engineering
Drexel University
Philadelphia, 19104 PA, USA

Prof. M. W. Barsoum
Department of Materials Science and Engineering
Drexel University
Philadelphia, 19104 PA, USA

The ORCID identification number(s) for the author(s) of this article can be found under https://doi.org/10.1002/adma.201706409.

DOI: 10.1002/adma.201706409

© 2018 WILEY-VCH Verlag GmbH & Co. KGaA, Weinheim

cheaper catalysts comprised of abundant materials are highly sought.[13] A range of earth abundant, inexpensive alternatives to Pt including sulfides, carbides, and phosphides have been developed with varying degrees of success.[14,15] Improved HER catalysts have the potential to enable large-scale transition to more renewable energy in the form of H_2, generated from electrochemical water splitting, that is, water electrolysis. A good HER catalyst is a stable material, with an optimal binding energy of adsorbed H_2.[16]

It follows that a particularly interesting application of MXenes is as catalysts in chemical or electrochemical reactions. For example, theoretical simulations suggest that MXene materials in general,[17] and the hypothetical W-based MXene, in particular,[9] can fulfill both of these crucial requirements. Recently, Pan used density functional theory (DFT) to calculate the H_2, adsorption free energy, ΔG_{ad}—a crucial material metric for HER—as a function of MXene composition and structure, and predicted that W_2C and Mo_2C should have high HER activity. The MXene, W_2C, in particular, was predicted to have HER activity rivaling that of Pt as the coverage dependent ΔG_{ad} approaches thermoneutral.[9]

Along the same lines there are several important characteristics that set MXenes apart from other materials. They include: (1) thermal and electrochemical stability, (2) intrinsic metallic conductivity, making the entire surface of the 2D material, as well as the edges, HER active, and (3) precise control of surface atomic structures and compositions. Indeed, in a recent report, detailed experimental evaluation of Mo_2CT_x MXene showed a high activity for HER, indicating that MXene materials have great potential in this domain.[18]

Inspired by the above, we use predictive phase stability theory to search for W-based MAX and *i*-MAX phases. The latter are quaternary MAX phases with the general formula $(M^1_{2/3}M^2_{1/3})_2AlC$, where M^1 and M^2 are two different early transition metals. What renders the *i*-MAX phases unique and the reason they are so called is because the M^1 and M^2 elements are ordered in the basal planes.[19,20] They are thus fundamentally different from the out-of-plane ordered (*o*-MAX) phases.[21,22] The discovery of the *i*-MAX phases is quite recent.[19,20] The first was $(Mo_{2/3}Sc_{1/3})_2AlC$, followed by $(V_{2/3}Zr_{1/3})_2AlC$ and $(Mo_{2/3}Y_{1/3})_2AlC$.[19,20] What renders the *i*-MAX phases particularly fascinating is that—depending on the severity of the etching solution—they can be transformed to either $(M^1_{2/3}M^2_{1/3})_2C$ or $M^1_{1.33}C$ MXenes. A schematic of the *i*-MAX to MXene transformation is shown in **Figure 1**. The fact that the vacancies in the $M^1_{1.33}C$ MXenes are ordered (see top right panel in Figure 1), is an unprecedented advantage that can be further used to tailor properties.

Herein, we not only report on two new W-based *i*-MAX phases, but also we show how etching these solids results in 2D $W_{1.33}C$ MXenes with ordered vacancies. We also evaluate the HER activity through electrochemical experiments. The results show that the *i*-MAX phases can lead to novel MXene chemistries beyond traditionally known M elements. Furthermore, the W-based MXene is experimentally found to be a new and quite promising catalyst for HER. Crucially this is the first report on a W-containing MAX phase of any kind, let alone one in which the M-elements are in-plane ordered. With this work we added a new element, W, to the MAX-phase family, and, we made, again for the first time, a W-based MXene.

The first task was to probe the compositional space of the ternary W-based MAX phases, W_2AC, and quaternary *i*-MAX phases, $(W_{2/3}M^1_{1/3})_2AlC$, where M^1 = Sc and Y, and A = Al, Si, Ga, Ge, In, and Sn. To that effect we used first-principles calculations based on DFT (see the Experimental Section). A compound's stability is quantified in terms of the formation enthalpy, ΔH_{cp}, by comparing its energy to the energy of a linear combination of competing phases resulting in the lowest energy, also called the equilibrium simplex. Said otherwise

$$\Delta H_{cp} = E(\text{compound}) - E(\text{equilibrium simplex}) \quad (1)$$

If $\Delta H_{cp} < 0$ the compound is considered stable, while for $\Delta H_{cp} > 0$ it is considered not stable or at best metastable. Our results are shown in **Table 1**.

From the results it is obvious that none of the ternary W-based MAX phases (columns 4 and 5 in Table 1) are stable, which explains why none have ever been reported. Out of 12 different chemically ordered *i*-MAX phases, two—$(W_{2/3}Sc_{1/3})_2AlC$ and $(W_{2/3}Y_{1/3})_2AlC$—are stable, with formation enthalpies of −27 and −22 meV/atom, respectively. This result is comparable to the formation enthalpy of known ternary MAX phases.[23,24] As for other *i*-MAX phases, the monoclinic (C2/c, No. 15) and orthorhombic (Cmcm, No. 63) structures are found almost degenerate in energy, see Figure S1 and Table S1 (Supporting Information). The identified equilibrium simplex for each MAX and *i*-MAX phase is shown in Tables S2–S4 (Supporting Information) and all competing phases are listed in Table S5 (Supporting Information). Furthermore, the calculated phonon dispersions of the $(W_{2/3}Sc_{1/3})_2AlC$ and $(W_{2/3}Y_{1/3})_2AlC$ phases, in

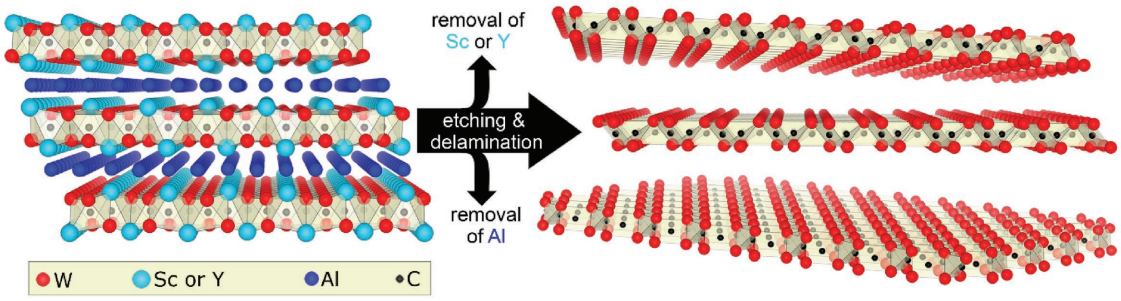

Figure 1. Schematic showing in-plane chemical ordering in $(W_{2/3}Sc_{1/3})_2AlC$ or $(W_{2/3}Y_{1/3})_2AlC$ *i*-MAX phase (left panel), leading to $W_{1.33}C$ MXene with ordered divacancies after selective etching and delamination (right panel).

© 2018 WILEY-VCH Verlag GmbH & Co. KGaA, Weinheim

Table 1. Calculated formation enthalpies, ΔH_{cp} for W_2AC, $(W_{2/3}Sc_{1/3})_2AC$, and $(W_{2/3}Y_{1/3})_2AC$ phases with A from group 13 (Al, Ga, In) and 14 (Si, Ge, Sn).

Period	A-element		ΔH_{cp} [meV/atom]					
	Group		W_2AC		$(W_{2/3}Sc_{1/3})_2AC$		$(W_{2/3}Y_{1/3})_2AC$	
			Group		Group		Group	
	13	14	13	14	13	14	13	14
3	Al	Si	+148	+295	−27	+106	−22	+82
4	Ga	Ge	+164	+241	+23	+66	+49	+169
5	In	Sn	+320	+366	+95	+134	+131	+235

the C2/c structure, are shown in Figure S2 (Supporting Information). The absence of imaginary frequencies indicates that both phases are dynamically stable, that is, stable with respect to lattice vibrations.

Scanning transmission electron microscopy (STEM) images of the *i*-MAX phase $(W_{2/3}Sc_{1/3})_2AlC$ along [010], [100], and [110] zone axes are shown, respectively, in **Figure 2**A–C, with the corresponding selective area electron diffraction (SAED) shown in Figure 2D–F. In these microscopy images, the W atoms appear bright; the Sc and Al atoms are less bright. The schematics show the atomic arrangements expected assuming monoclinic a C2/c structure. In Figure 2B, the structure looks identical to a

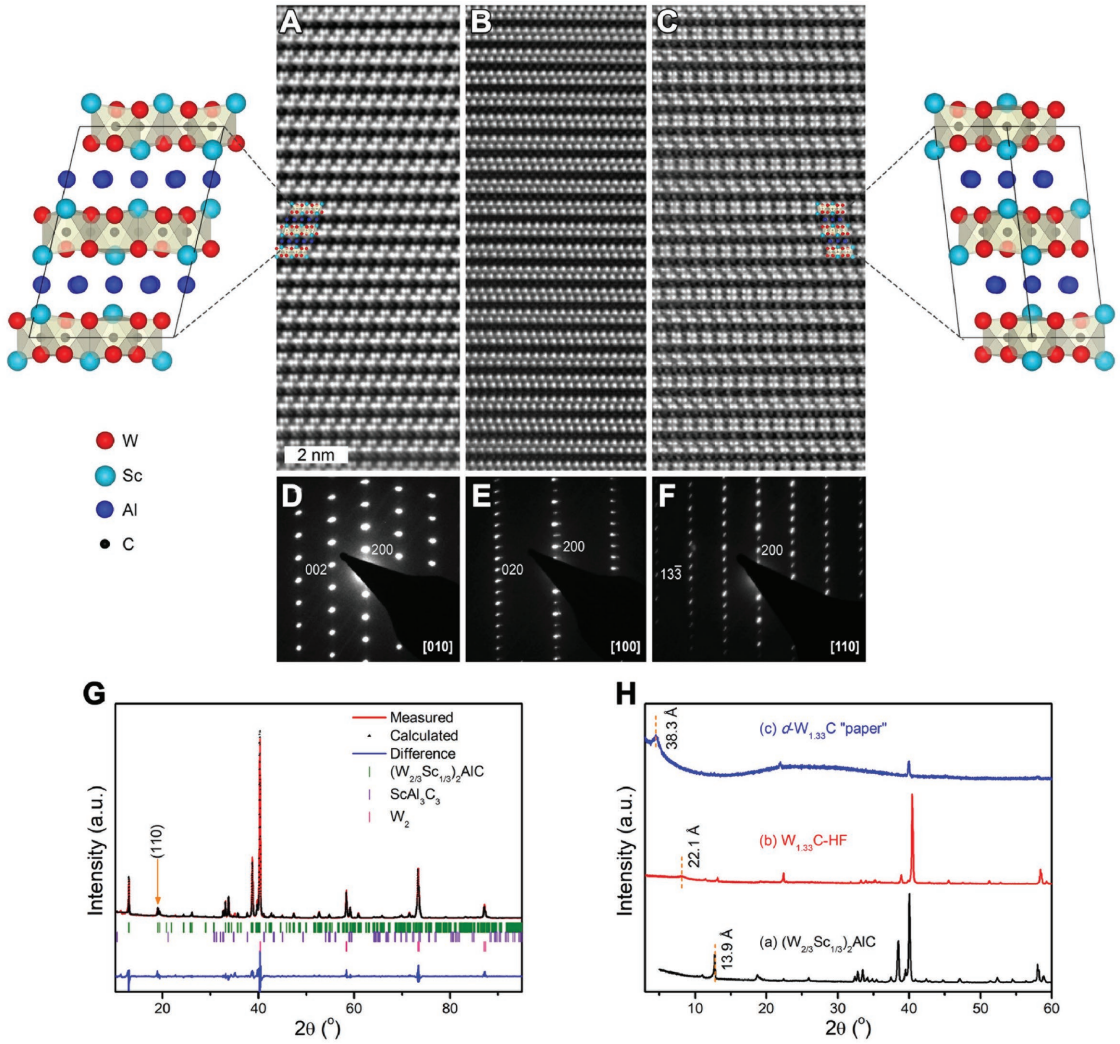

Figure 2. The HRSTEM images, and corresponding schematic representations of $(W_{2/3}Sc_{1/3})_2AlC$, are shown along the A) [010], B) [100], and C) [110] zone axes, D–F) with corresponding SAED. Schematics on right and left are based on the identified monoclinic structure of space group C2/c. G) XRD pattern and Rietveld refinement for a sample of nominal composition $(W_{2/3}Sc_{1/3})_2AlC$. H) XRD pattern of $(W_{2/3}Sc_{1/3})_2AlC$, a) before etching, b) after HF etching, and c) after etching, followed by TBAOH intercalation and delamination.

© 2018 WILEY-VCH Verlag GmbH & Co. KGaA, Weinheim

traditional MAX phase viewed along the [11$\bar{2}$0] zone axis. However, evidence for in-plane ordering of the two transition metals is revealed in Figure 2A,C, respectively, with an atomic stacking ruling out orthorhombic symmetry (Figure S1, Supporting Information). Note that, like in previous work, the Sc atoms extend out of the W planes toward the Al layers.[19,20] The in-plane ordered structure is also supported by SAED. Also in line with previous work, the Al layers consequently form a Kagomé-like lattice, evident from the bright–dark contrast variation in that layer.[20] Local energy-dispersive X-ray (EDX) spectroscopy reveals a W:Sc:Al ratio (in at%) of 45:25:30, which, within error bars, is consistent with the predicted W:Sc ratio of 2:1.

Figure 2G shows a powder X-ray diffraction (XRD) pattern of a $(W_{2/3}Sc_{1/3})_2AlC$ sample including Rietveld refinement based on a C2/c structure (No. 15). The refinement parameters are listed in Table S6 (Supporting Information). The sample contains ≈43 wt% $(W_{2/3}Sc_{1/3})_2AlC$, with refined lattice parameters of a = 9.368, b = 5.404, and c = 13.960 Å, which is close to our theoretically predicted parameters of the monoclinic structure of 9.327, 5.398, and 13.969 Å, respectively. Impurity phases in the sample are ≈26 wt% $ScAl_3C_3$ and unreacted ≈31 wt% W. Note that while the material before etching is not single phase, after etching it is (see below). It should also be stressed that the (110) peak (shown by arrow in Figure 2G) which is due to the W/Sc in-plane chemical ordering and characteristic of *i*-MAX phases, can be found around 19° 2θ.[20]

The W-based *i*-MAX phase can be used as a parent material for a pure W-based MXene. Figure 2H shows the XRD patterns of $(W_{2/3}Sc_{1/3})_2AlC$, (a) before etching and (b) after etching in a 48% hydrofluoric acid (HF) solution. The etching increases the *c*-lattice parameter, *c*-LP, from 13.96 to 22.16 Å due to the presence of extra water and cations between the $W_{1.33}CT_x$ layers.[25] To create a colloidal solution for further use, the MXene multilayers are intercalated with tetrabutylammonium hydroxide (TBAOH), after which the MXene flakes delaminate spontaneously in water to form *d*-$W_{1.33}C$.[26] To produce freestanding, binder-free "paper" or films (Figure S3A, Supporting Information), the colloidal solution was filtered through a nanoporous membrane. A typical XRD pattern of the "paper" (Figure 2H (c)) shows a broad peak around 5°, which corresponds to a *c*-LP of 38.3 Å. This value is typical of MXenes intercalated with TBAOH.[26]

The absence of Al and Sc, as evidenced by EDX of this film (Figure S3A, Supporting Information), implies that our final MXene composition is $W_{1.33}C$. It is important to note that $(W_{2/3}Sc_{1/3})_2AlC$ can also be transformed into its MXene by etching in a LiF/HCl solution (Figure S4A, Supporting Information). Here, again, the Al and Sc atoms are selectively etched. For further information on MXene vacancy formation and chemical bonding, see Sections S1 and S2 (Supporting Information).

Based on the results shown in Table 1, $(W_{2/3}Y_{1/3})_2AlC$ should also exist, as indeed observed. STEM images and corresponding schematics of this phase are shown in **Figure 3**A–C, viewed in the (A) [010], (B) [100], and (C) [110] direction, respectively. SAED along the [010], [100], and [110] zone axes are shown in Figure 3D–F, which along with the STEM images support a monoclinic C2/c *i*-MAX structure. In these images, the W atoms appear bright, while the Y and Al atoms are less bright. In-plane ordering of W and Y (extending toward the Al layer) as well as indications of a Kagomé-like lattice in the Al layer, can be concluded in line with the results for $(W_{2/3}Sc_{1/3})_2AlC$. STEM-EDX shows a W:Y ratio of 51:24, confirming the simulated and intended 2:1 *i*-MAX chemistry.

Figure 3G shows a powder XRD pattern of $(W_{2/3}Y_{1/3})_2AlC$ including Rietveld refinement based on a C2/c structure (No. 15), as well as a Cmcm structure (No. 63). Out of about ten regions investigated with STEM, only one showed a structure characteristic of Cmcm (see Figure S5, Supporting Information), however, in the XRD refinement process, there are strong indications of substantial amounts of a phase with space group No. 63. The refinement parameters are listed in Tables S7 and S8 (Supporting Information), suggesting lattice parameters of the C2/c structure of a = 9.51, b = 5.49, and c = 14.22 Å, to be compared to our theoretically predicted parameters for the monoclinic structure of 9.544, 5.519, and 14.128 Å, respectively. The phase composition from the refinement suggests that the sample also contains ≈32.1 wt% $(W_{2/3}Y_{1/3})_2AlC$ belonging to space group 63 (*Cmcm*), with refined lattice parameters of a = 9.52, b = 5.50, and c = 13.67 Å, and the impurity phases YAl_3C_3 (≈31.4 wt%), W (≈18.0 wt%), and Y_2O_3 (≈4.5 wt%).

Not surprisingly, $(W_{2/3}Y_{1/3})_2AlC$ can also be converted to a W-based MXene. Figure 3H shows the XRD patterns of $(W_{2/3}Y_{1/3})_2AlC$, (a) before etching, (b) after etching in HF, and (c) after etching, intercalating with TBAOH and filtering of the resulting colloidal solution. In this case, the *c*-LP increases from 13.7 Å for the *i*-MAX phase, to 18.3 and 26.1 Å for the multilayer powders and MXene "paper" (see Figure S3C, Supporting Information), respectively. From EDX results of this filtered film (Figure S3D, Supporting Information), we conclude that both the Al and Y atoms were etched. It follows that, here again, the end product is a pure WC-based MXene. The same end result can be obtained by etching $(W_{2/3}Y_{1/3})_2AlC$ in a LiF/HCl solution (Figure S4B, Supporting Information).

A typical STEM image of single, and folded, $W_{1.33}C$ flakes is shown in **Figure 4**A. A medium magnification image (Figure 4B) and corresponding fast Fourier transform (FFT) (inset in Figure 4B) reveal a hexagonal crystal structure. The outer hexagonal pattern of the FFT corresponds to the in-plane interatomic distances, while the inner hexagonal pattern is the result of the symmetry formed by the ordered vacancies. This symmetry was established in our previous work.[19] The corresponding, almost identical, results for $W_{1.33}C$ flakes obtained by etching $(W_{2/3}Y_{1/3})_2AlC$ are shown in Figure S6 (Supporting Information).

Guided by Pan,[9] and DFT calculations that predicted high catalytic activity of W-containing MXenes, we decided to test how active $W_{1.33}CT_x$ was for HER. To place the results in perspective we compared them with results for $Mo_{1.33}C$—another MXene with ordered vacancies[19]—and a Pt/carbon electrode. The results, presented in Figure 4D, show that the HER activity—as indicated by an overpotential-dependent current density, measured thorough potentiodynamic polarization curves—for as-received $W_{1.33}C$ MXenes is rather poor. This is attributed to the oxophilicity of W, which leads to partial oxidation of the MXene in the as-received form. However, after annealing in Ar-based forming gas (1 h at 700 °C in H_2(3%)/Ar), the surface O/OH coverage is reduced and a significant

© 2018 WILEY-VCH Verlag GmbH & Co. KGaA, Weinheim

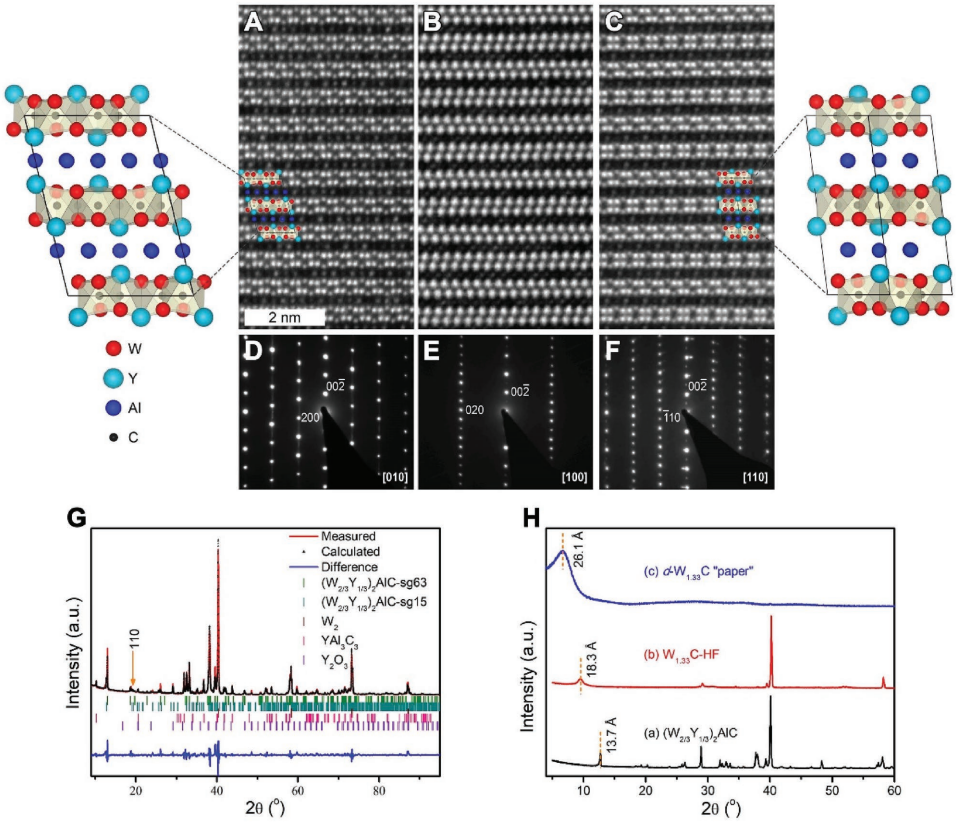

Figure 3. The high-resolution microscopy images and corresponding schematic representations are shown along the A) [010] and B) [100], and C) [110] direction. SAED is shown along the D) [010], E) [100], and F) [110] zone axis, confirming the identified monoclinic structure of space group C2/c. G) XRD pattern and Rietveld refinement for a sample of nominal composition $(W_{2/3}Y_{1/3})_2$AlC. H) XRD pattern of $(W_{2/3}Y_{1/3})_2$AlC a) before etching, b) after HF etching, and c) after etching, followed by TBAOH intercalation, and delamination to create freestanding "paper."

improvement in HER activity is observed (compare dashed and solid red lines in Figure 4D). The overpotential of the annealed MXene was a very respectable ≈320 mV at a current density of 10 mA cm^{-2}. Also clear is that all MXenes are catalytically active for the HER with activity increasing in the order $W_{1.33}C$ (unannealed) < $Mo_{1.33}C$ < $W_{1.33}C$ (annealed). This trend is likely related to the structure and compositional-dependent H_2 adsorption free energy on the MXenes, as well as the average valance state of the surface.[9]

Theoretical predictions show that surface treatment of MXenes, such as oxidization or hydrogenation, is critical to enhance the catalytic performance.[9] It is worth noting that the theoretical calculations were carried out on W_2C, whereas herein $W_{1.33}CT_x$ was tested. The instability of W_2AlC precludes the synthesis of W_2C (Table 1). That said, the initial results are quite promising and provide insight for further activity improvements through optimization of surface functionalizations, atomic structure, material compositions, and electrode architectures.

The implications and ramification of the results obtained herein cannot be overemphasized for several reasons. Chief among them is a methodology to synthesize MXenes with elements that cannot be synthesized otherwise. Herein, we show that W_2AlC is very far from being stable (Table 1) rendering it impossible to make W_2CT_x. However, by showing that not only are $(W_{2/3}Sc_{1/3})_2$AlC and $(W_{2/3}Y_{1/3})_2$AlC stable, both theoretically and experimentally, but that both can be used to synthesize $W_{1.33}C$, the impossible is rendered partially possible. In all previous work on MXene, the chemistries obtained were those of the group of M element forming MAX phases discovered by Nowotny almost half a century ago.[2,27] More specifically, all MXene synthesized to date are comprised of Ti, V, Cr, Zr, Nb, Mo, Hf, and/or Ta. The present work adds one more very important element: W. In due time it is reasonable to assume that our approach will add many other elements, greatly expanding the already prolific compositional space of MXenes. That our approach also expands the MAX compositional space, that numbers more than 70 to date, is noteworthy and of great importance[2] by itself. The MAX phases are an important class of layered carbides and nitrides with great potential in many applications.[2]

Furthermore, point defects in general, and vacancies in particular, are known to impact the electric, magnetic, optoelectronic, catalytic, etc., properties of 2D materials.[28–30] Admittingly, for this work it would have been advantageous to test the catalytic activity of W_2C, but the fact that we readily form a $W_{1.33}C$ 2D material with ordered divacancies will indubitably shine in catalytic reactions and other applications. Consequently, these MXenes allow for the exploration of uncharted territory that should lead to unique and diverse properties.

In conclusion, two new W-based *i*-MAX phases, $(W_{2/3}Sc_{1/3})_2$AlC and $(W_{2/3}Y_{1/3})_2$AlC, were predicted and

© 2018 WILEY-VCH Verlag GmbH & Co. KGaA, Weinheim

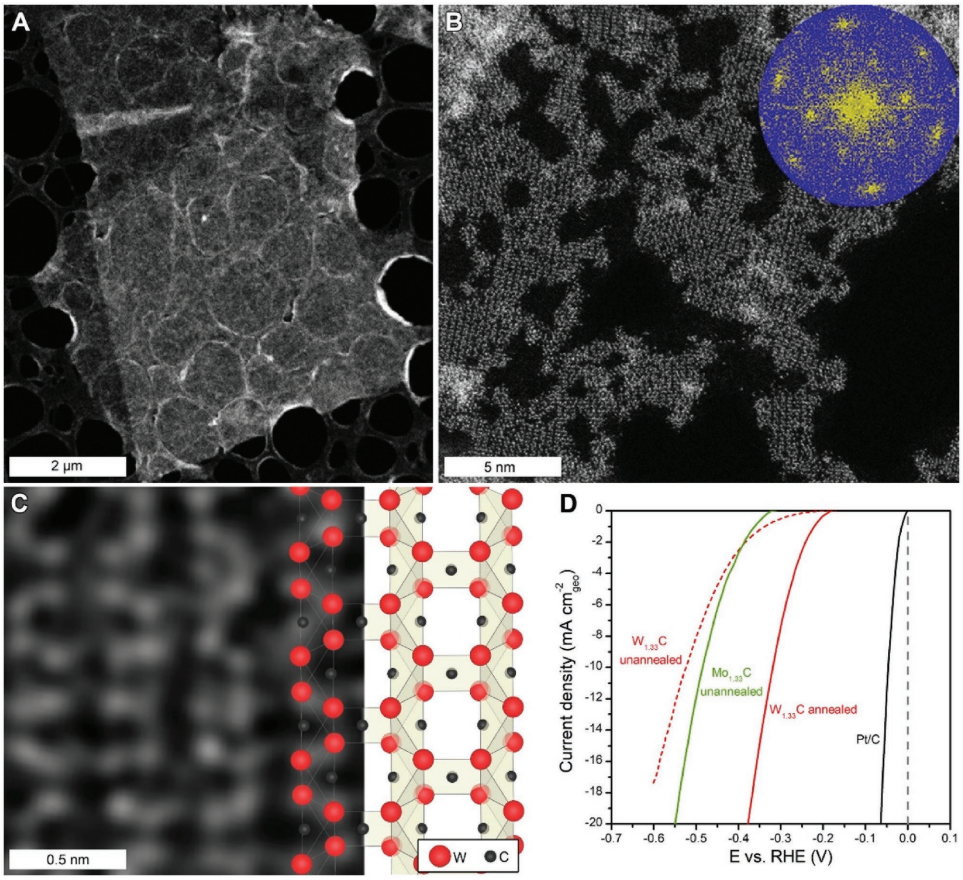

Figure 4. A–C) Top view of HAADF-STEM of single $W_{1.33}C$ sheets with ordered divacancies obtained from parent $(W_{2/3}Sc_{1/3})_2AlC$. A) Low-magnification image of single flake with lateral dimensions > 5 μm. B) Higher magnification image with corresponding FFT (shown in inset). C) Atomically resolved image with overlaid schematic atomic structure model. D) HER polarization curves for $Mo_{1.33}C$ (green), unannealed $W_{1.33}C$ (dashed red), annealed $W_{1.33}C$ (red), and Pt/C (black) recorded in H_2 saturated 0.1 M $HClO_4$ at room temperature with a rotation rate of 1600 rpm and a potential sweep rate of 50 mV s^{-1}. Catalyst loading on the GC disk for $Mo_{1.33}C$ and $W_{1.33}C$ was 0.1 mg cm^{-2}. Pt/C loading is 12 μg_{Pt} cm^{-2}. All potentials are corrected for *iR* drop in the electrolyte.

experimentally synthesized. By selectively etching the Sc/Y and Al atoms these *i*-MAX phases were converted to pure W-based MXenes, the first of its type. The latter have ordered basal-plane vacancies. Initial HER activity results of this MXene point toward its great potential as a catalyst material for hydrogen-energy technologies.

Experimental Section

Theoretical Calculations: All first-principles calculations based on DFT were performed with the Vienna ab initio simulation package (VASP)[31–33] using the projector augmented wave method[34,35] with non-spin-polarized generalized gradient approximation (GGA) as parameterized by Perdew–Burke–Ernzerhof (PBE)[36] for treating electron exchange and correlation effects. Wave functions were expanded in plane waves up to an energy cutoff of 400 eV. Sampling of the Brillouin zone was done using the Monkhorst–Pack scheme with a *k*-point grid, ensuring energy convergence within 0.1 meV, for example, for $(W_{2/3}M^2_{1/3})_2AC$ a 7 × 13 × 5 *k*-point grid was used.[37] All structures were relaxed until the forces on all atoms converged to below 10^{-5} eV $Å^{-1}$. The thermodynamic stability was evaluated using a linear optimization procedure based on the simplex method, which compares the energy of the compound of interest to all possible linear combinations of other competing phases under the constraint of a fixed stoichiometry.[24,38] Temperature-dependent effects such as lattice vibrations were not considered, as such contribution from a phase, significant or not, tend to be cancelled out in the calculated stability.[39] This approach was proven to work exceptionally well for MAX phases.[24,40,41] Competing phases included in the evaluation of phase stability are those experimentally known as well as hypothetical phases that exist in similar and/or with neighboring elements in the periodic table of elements. A complete list of competing phases considered herein is given in Table S5 (Supporting Information). Schematics were produced with VESTA.[42]

Dynamical stability, in terms of phonon dispersion, was calculated for $(W_{2/3}Sc_{1/3})_2AlC$ and $(W_{2/3}Y_{1/3})_2AlC$, with the C2/c structure, from 2 × 3 × 2 supercells, using the finite displacement method as implemented in Phonopy.[43]

Materials Synthesis: Elemental powders of W (12 μm, Sigma-Aldrich), Sc (–200 mesh Stanford Advanced Material), Al and C (–200 mesh Alfa Aesar), were mixed in desired stoichiometric ratios and placed in a covered Al_2O_3 crucible. The latter was placed in an alumina tube furnace—through which Ar was flowing—heated at a rate of 8 °C min^{-1} to 1450 °C, and held at that temperature for 2 h. After cooling, the lightly sintered sample was crushed in an agate mortar, resulting in a fine $(W_{2/3}Sc_{1/3})_2AlC$ powder. A similar procedure was carried out for the synthesis of $(W_{2/3}Y_{1/3})_2AlC$, where the same W, Al, and graphite powders together with elemental Y powders (with a particle size of –40 mesh) were mixed and sintered at 1450 °C for 2 h.

Structural/Compositional Characterization: For structural characterization of the phases, (θ–2θ) XRD on the powders were

© 2018 WILEY-VCH Verlag GmbH & Co. KGaA, Weinheim

performed using a PANalytical X'Pert powder diffractometer, with Cu source ($\lambda_{K_\alpha} \approx 1.54$ Å). The optics utilized for these measurements were a graded Bragg–Brentano HD with a 1/4° divergent and ½° antiscattered slits, in the incident beam side, and a 5 mm antiscatter slit together with a Soller slit (with an opening rad. of 0.04) in the diffracted beam side. A 5°–120° continuous scan was performed on the sample using a step size of 0.008° with a 40 s time per step. The XRD scans for both *i*-MAX samples were analyzed by Rietveld refinement using the FULLPROF code.[44] The fitting parameters utilized in the program were five backgrounds parameters, scale factor, *X* and *Y* profile parameter to limit the peak width to the major phase, lattice parameters, atomic positions, and occupancies for all phases and overall B-factors. Additional structural characterization, as well as compositional analysis was performed using transmission electron microscopy (TEM). For that purpose, high-resolution scanning transmission electron microscopy (HRSTEM), and EDX spectroscopy were carried out with Linköping's double C_s corrected FEI Titan^3 60-300 operated at 300 kV, and equipped with the Super-X EDX system. For further compositional analysis, and to study the morphology of the $W_{1.33}C$ MXenes paper, as well as measuring their thickness, a scanning electron microscope (SEM) was utilized using Linköping's SEM LEO 1550 Gemini, with an acceleration voltage between 5 and 10 keV, equipped with EDX.

MXene Synthesis: MXene samples were synthesized by two different methods, where in the first method—henceforth referred to as the HF method—≈1 g of *i*-MAX powders was added to ≈20 mL 48% aqueous HF, and stirred using a Teflon-coated magnetic stirrer for ≈30 h at room temperature. Afterward, the mixture was washed with, deionized, DI, water that was de-aerated with N_2 for 1 h. Washing was done by adding 10 mL of the de-aerated water to the etched powder, shaking manually for 1 min then centrifuging at 5000 rpm for 1 min. This process was repeated till the mixture pH was ≈5–6.

The produced multilayered MXene was delaminated via intercalation by adding ≈1 g of the powder into ≈5 mL of an organic base, TBAOH, which was then manually shaken for ≈5 min. The solution was put in centrifuge for another 5 min at 5000 rpm and was rinsed by DI de-aerated water three times without shaking to remove any TBAOH residues. Finally, the intercalated 1 g of the MXene powders was mixed with 5 mL of DI de-aerated water, manually shaken for 5 min, then centrifuged at 3000 rpm for 1 h.

The second method—henceforth referred to as LiF+HCl method—was carried out by adding 2 g of the powders to 4 g of lithium fluoride (LiF) dissolved in 60 mL of 12 M hydrochloric acid (HCl) and stirred using Teflon-coated magnetic stirrers for 48 h at 35 °C. The etching container was placed in a silicone-based oil bath. After etching, the mixture was washed three times with 12 M HCl, each time 50 mL of HCl was added to the MXene powders, manually shaken for 1 min, followed by 1 min of centrifugation at 5000 rpm. This step was carried out to remove any residual LiF. The MXene was then washed with 50 mL of 1 M LiCl solution three times. During each wash, the mixture was manually shaken for 1 min followed by centrifuging for 1 min at 5000 rpm after which the supernatant was decanted. This step was performed to re-intercalate Li ions in the MXene which may have been removed during the HCl washing. Finally, the MXene powders were washed with 50 mL DI de-aerated water until delamination occurs; this usually required 7–10 washes. In between each wash, the mixture was manually shaken for 5 min and centrifuged afterward for 1 min at 2000 rpm. After delamination, the suspension was centrifuged for 5 min at 2000 rpm.

Electrochemical Experiments: HER activity was measured through polarization curves recorded in a standard three-electrode electrochemical cell using a rotating disk electrode (RDE) setup (Pine Research Instrumentation) at room temperature and a rotation rate of 1600 rpm. Current/potential measurements were made with a potentiostat (Metrohm Autolab, PGSTAT302N). The colloidal MXene solution was diluted with ultrapure water through sonication to form a colloidal solution. The MXene suspension was then drop-cast onto a glassy carbon (GC) disk (5 mm diameter, SIGRADUR G from HTW Hochtemperatur-Werkstoffe GmbH) substrate, dried under flowing Ar, and mounted in the RDE rotator. Following loading on the GC, the $W_{1.33}C$ was annealed at 700 °C in H_2(3%)/Ar for 1 h. A commercial standard Pt/C (20 wt%, HiSPEC 3000) was tested at a loading of 12 μg_{Pt} cm^{-2}. The counter electrode was a graphite rod (3 mm diameter, Sigma Aldrich) and the reference electrode was Ag/AgCl (BASi). All potentials reported herein were converted to the reversible hydrogen electrode (RHE) scale. HER polarization curves were recorded in H_2-saturated 0.1 M $HClO_4$ prepared from concentrated $HClO_4$ (OmniTrace Ultra, Millipore) and 18.2 MΩ cm Milli-Q water. The samples were cycled until a stable CV was obtained and the anodic scan was used to evaluate the HER activity for all samples. All potentials were corrected for *iR* drop as determined from electrochemical impedance spectroscopy (EIS) analysis before the HER measurements. Details on HER durability testing, overpotential as a function of loading on the GC disk, polarization curve, electrochemical capacitance, and capacitance currents from CVs as a function of scan rate, for the annealed $W_{1.33}C$, are shown in Figures S8–S11 (Supporting Information).

Supporting Information

Supporting Information is available from the Wiley Online library or from the author.

Acknowledgements

The authors acknowledge the Swedish Research Council for funding under Grant Nos. 642-2013-8020 and 2016-04412, and the Knut and Alice Wallenberg Foundation for support of the electron microscopy laboratory in Linköping, a Fellowship and Project grant (KAW 2015.0043). The authors also acknowledge Swedish Foundation for Strategic Research (SSF) through the Synergy Grant FUNCASE, and the Research Infrastructure Fellow Program No. RIF 14-0074. The calculations were carried out using supercomputer resources provided by the Swedish National Infrastructure for Computing (SNIC) at the National Supercomputer Centre (NSC) and the High Performance Computing Center North (HPC2N). National Science Foundation through the Catalysis Program in the Division of Chemical, Biological, Environmental and Transport Systems, under Award No. 1602886.

Conflict of Interest

The authors declare no conflict of interest.

Keywords

density functional theory, hydrogen evolution reaction, *i*-MAX phase, MXene, tungsten

Received: November 3, 2017
Revised: December 20, 2017
Published online:

[1] S. Z. Butler, S. M. Hollen, L. Cao, Y. Cui, J. A. Gupta, H. R. Gutiérrez, T. F. Heinz, S. S. Hong, J. Huang, A. F. Ismach, E. Johnston-Halperin, M. Kuno, V. V. Plashnitsa, R. D. Robinson, R. S. Ruoff, S. Salahuddin, J. Shan, L. Shi, M. G. Spencer, M. Terrones, W. Windl, J. E. Goldberger, *J. Am. Chem. Soc.* **2013**, *7*, 2898.

[2] M. W. Barsoum, *MAX Phases: Properties of Machinable Ternary Carbides and Nitrides*, Wiley-VCH, Weinheim, Germany **2013**.

© 2018 WILEY-VCH Verlag GmbH & Co. KGaA, Weinheim

[3] M. W. Barsoum, *Prog. Solid State Chem.* **2000**, *28*, 201.
[4] B. Anasori, M. R. Lukatskaya, Y. Gogotsi, *Nat. Rev. Mater.* **2017**, *2*, 16098.
[5] Q. Peng, J. Guo, Q. Zhang, J. Xiang, B. Liu, A. Zhou, R. Liu, Y. Tian, *J. Am. Chem. Soc.* **2014**, *136*, 4113.
[6] F. Shahzad, M. Alhabeb, C. B. Hatter, B. Anasori, S. Man Hong, C. M. Koo, Y. Gogotsi, *Science* **2016**, *353*, 1137.
[7] J. Halim, K. M. Cook, M. Naguib, P. Eklund, Y. Gogotsi, J. Rosen, M. W. Barsoum, *Appl. Surf. Sci.* **2016**, *362*, 406.
[8] H. Weng, A. Ranjbar, Y. Liang, Z. Song, M. Khazaei, S. Yunoki, M. Arai, Y. Kawazoe, Z. Fang, X. Dai, *Phys. Rev. B* **2015**, *92*, 075436-1,075436-7.
[9] H. Pan, *Sci. Rep.* **2016**, *6*, 32531.
[10] H. Fang, S. Chuang, T. C. Chang, K. Takei, T. Takahashi, A. Javey, *Nano Lett.* **2012**, *12*, 3788.
[11] A. Allain, J. Kang, K. Banerjee, A. Kis, *Nat. Mater.* **2015**, *14*, 1195.
[12] T. Georgiou, R. Jalil, B. D. Belle, L. Britnell, R. V. Gorbachev, S. V. Morozov, Y. J. Kim, A. Gholinia, S. J. Haigh, O. Makarovsky, L. Eaves, L. A. Ponomarenko, A. K. Geim, K. S. Novoselov, A. Mishchenko, *Nat. Nanotechnol.* **2013**, *8*, 100.
[13] X. Zou, Y. Zhang, *Chem. Soc. Rev.* **2015**, *44*, 5148.
[14] P. C. Vesborg, B. Seger, I. Chorkendorff, *J. Phys. Chem. Lett.* **2015**, *6*, 951.
[15] V. R. Stamenkovic, D. Strmcnik, P. P. Lopes, N. M. Markovic, *Nat. Mater.* **2016**, *16*, 57.
[16] Z. W. Seh, J. Kibsgaard, C. F. Dickens, I. Chorkendorff, J. K. Norskov, T. F. Jaramillo, *Science* **2017**, *355*, eaad4998.
[17] a) G. Gao, A. P. O'Mullane, A. Du, *ACS Catal.* **2016**, *7*, 494; b) C. Ling, L. Shi, Y. Ouyang, Q. Chen, J. Wang, *Adv. Sci.* **2016**, *3*, 1600180.
[18] Z. W. Seh, K. D. Fredrickson, B. Anasori, J. Kibsgaard, A. L. Strickler, M. R. Lukatskaya, Y. Gogotsi, T. F. Jaramillo, A. Vojvodic, *ACS Energy Lett.* **2016**, *1*, 589.
[19] Q. Tao, M. Dahlqvist, J. Lu, S. Kota, R. Meshkian, J. Halim, J. Palisaitis, L. Hultman, M. W. Barsoum, P. O. A. Persson, J. Rosen, *Nat. Commun.* **2017**, *8*, 14949.
[20] M. Dahlqvist, J. Lu, R. Meshkian, Q. Tao, L. Hultman, J. Rosen, *Sci. Adv.* **2017**, *3*, e1700642.
[21] B. Anasori, M. Dahlqvist, J. Halim, E. J. Moon, J. Lu, B. C. Hosler, E. a. N. Caspi, S. J. May, L. Hultman, P. Eklund, J. Rosén, M. W. Barsoum, *J. Appl. Phys.* **2015**, *118*, 094304.
[22] Z. Liu, E. Wu, J. Wang, Y. Qian, H. Xiang, X. Li, Q. Jin, G. Sun, X. Chen, J. Wang, M. Li, *Acta Mater.* **2014**, *73*, 186.
[23] V. J. Keast, S. Harris, D. K. Smith, *Phys. Rev. B* **2009**, *80*, 214113.
[24] M. Dahlqvist, B. Alling, J. Rosén, *Phys. Rev. B* **2010**, *81*, 220102.
[25] M. Ghidiu, M. R. Lukatskaya, M.-Q. Zhao, Y. Gogotsi, M. W. Barsoum, *Nature* **2014**, *516*, 78.
[26] M. Naguib, M. Kurtoglu, V. Presser, J. Lu, J. Niu, M. Heon, L. Hultman, Y. Gogotsi, M. W. Barsoum, *Adv. Mater.* **2011**, *23*, 4248.
[27] H. Nowotny, *Prog. Solid State Chem.* **1971**, *5*, 27.
[28] A. W. Robertson, C. S. Allen, Y. A. Wu, K. He, J. Olivier, J. Neethling, A. I. Kirkland, J. H. Warner, *Nat. Commun.* **2012**, *3*, 1144.
[29] Y. Liu, H. Xiao, W. A. Goddard III, *Nano Lett.* **2016**, *16*, 3335.
[30] M. Amani, D.-H. Lien, D. Kiriya, J. Xiao, A. Azcatl, J. Noh, S. R. Madhvapathy, R. Addou, S. KC, M. Dubey, K. Cho, R. M. Wallace, S.-C. Lee, J.-H. He, J. W. Ager III, X. Zhang, E. Yablonovitch, A. Javey, *Science* **2015**, *350*, 1065.
[31] G. Kresse, J. Hafner, *Phys. Rev. B* **1993**, *47*, 558.
[32] G. Kresse, J. Furthmiiller, *Comput. Mater. Sci.* **1996**, *6*, 15.
[33] G. Kresse, J. Furthmüller, *Phys. Rev. B* **1996**, *54*, 11169.
[34] P. E. Blöchl, *Phys. Rev. B* **1994**, *50*, 17953.
[35] G. Krasse, D. Joubert, *Phys. Rev. B* **1999**, *59*, 1758.
[36] J. P. Perdew, K. Burke, M. Ernzerhof, *Phys. Rev. Lett.* **1996**, *77*, 3865.
[37] H. J. Monkhorst, J. D. Pack, *Phys. Rev. B* **1976**, *13*, 5188.
[38] M. Dahlqvist, B. Alling, I. A. Abrikosov, J. Rosén, *Phys. Rev. B* **2010**, *81*, 024111.
[39] A. Thore, M. Dahlqvist, B. Alling, J. Rosén, *J. Comput. Mater. Sci.* **2014**, *91*, 251.
[40] P. Eklund, M. Dahlqvist, O. Tengstrand, L. Hultman, J. Lu, N. Nedfors, U. Jansson, J. Rosén, *Phys. Rev. Lett.* **2012**, *109*, 035502.
[41] A. S. Ingason, A. Petruhins, M. Dahlqvist, F. Magnus, A. Mockute, B. Alling, L. Hultman, I. A. Abrikosov, P. O. Å. Persson, J. Rosen, *Mater. Res. Lett.* **2014**, *2*, 89.
[42] K. Momma, F. Izumi, *J. Appl. Crystallogr.* **2011**, *44*, 1272.
[43] A. Togo, F. Oba, I. Tanaka, *Phys. Rev. B* **2008**, *78*, 134106.
[44] H. M. Rietveld, *J. Appl. Crystallogr.* **1969**, *2*, 65.

© 2018 WILEY-VCH Verlag GmbH & Co. KGaA, Weinheim